NASA TN D-1485

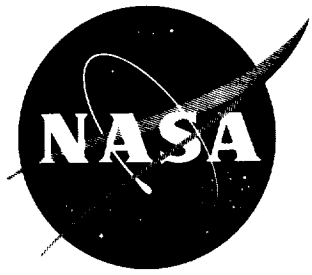

TECHNICAL NOTE

D-1485

EXPERIMENTAL INVESTIGATION AT MACH NUMBER 3.0 OF EFFECTS OF THERMAL STRESS AND BUCKLING ON FLUTTER CHARACTERISTICS OF FLAT SINGLE-BAY PANELS OF LENGTH-WIDTH RATIO 0.96

By Sidney C. Dixon

Langley Research Center
Langley Station, Hampton, Va.

NATIONAL AERONAUTICS AND SPACE ADMINISTRATION
WASHINGTON
November 1962

NATIONAL AERONAUTICS AND SPACE ADMINISTRATION

TECHNICAL NOTE D-1485

EXPERIMENTAL INVESTIGATION AT MACH NUMBER 3.0 OF EFFECTS OF THERMAL STRESS AND BUCKLING ON FLUTTER CHARACTERISTICS OF FLAT SINGLE-BAY PANELS OF LENGTH-WIDTH RATIO 0.96

By Sidney C. Dixon

SUMMARY

Flat, single-bay, skin stiffener panels with length-width ratios of 0.96 were tested at a Mach number of 3.0, at dynamic pressures ranging from 1,500 to 5,000 pounds per square foot, and at stagnation temperatures from 300° F to 660° F in order to investigate the effects of thermal stress and buckling on the flutter of such panels. The panel supporting structure allowed partial thermal expansion of the skins in both the longitudinal and lateral directions. Panel skin material and skin thickness were varied.

A boundary faired through the experimental flutter points consisted of a flat-panel portion, a buckled-panel portion, and a transition point, at the intersection of the two boundaries, where a panel is most susceptible to flutter. The flutter region consisted of two fairly distinct sections, a large-amplitude flutter region and a small-amplitude flutter region. The results show that an increase in panel skin temperature (or increase in thermal stress) makes a flat (unbuckled) panel more susceptible to flutter. The flutter trend for buckled panels is reversed. Use of a modified temperature parameter, which approximately accounts for the effects of differential pressure and variations in panel skin material and skin thickness, reduced the scatter in the data which resulted when these effects were neglected. The results are compared with an exact theory for clamped panels for the condition of zero midplane stress. In addition, a two-mode "transtability" solution for clamped panels is compared with the experimentally determined transition point.

INTRODUCTION

Flutter characteristics of thermally stressed panels have become important with the advent of sustained supersonic flight and the aerodynamic heating associated with such flight conditions. However, very little experimental information exists concerning the flutter behavior of panels acted upon by compressive forces, particularly in the nonbuckled range. Some information on the effects of midplane compressive stress has been obtained experimentally through mechanical buckling (with some heating) of clamped plates having length-width ratios of 5

or less. (See, for example, refs. 1 to 4.) In addition, the effects of compressive stress and buckling, induced by aerodynamic heating, on the flutter characteristics of multibay panels with length-width ratios of 10 have been reported in references 5 and 6.

The experimental flutter trends presented in references 5 and 6 revealed that the flutter boundary consists of a flat-panel portion, a buckled-panel portion, and a transition point, at the intersection of the two boundaries, where a panel is most susceptible to flutter. The flat-panel boundary indicated that, for a given panel and aerodynamic conditions, an increase in panel temperature (or midplane compressive stress in the direction of air flow) made a flat panel more susceptible to flutter; the experimental flutter trends for flat panels were similar to trends predicted theoretically in references 7, 8, and 9. For the buckled-panel boundary the trends were reversed; once a panel is thermally buckled, any additional temperature rise will tend to stiffen the panel.

The present investigation was conducted in the Langley 9- by 6-foot thermal structures tunnel and was undertaken to determine the effects of compressive stress (induced by aerodynamic heating) and buckling on the flutter characteristics of panels with length-width ratios of 0.96. Single-bay panels, 25.6 inches long and 26.6 inches wide, were tested at a Mach number of 3.0 at various dynamic pressures and stagnation temperatures. Panel skin material and skin thickness were varied. The panel-supporting structure was such that partial thermal expansion of the skin could occur in both the longitudinal and lateral directions and thus delay thermal buckling and permit more extensive study of the flat-panel flutter boundary.

The flutter data obtained in this investigation are presented in tabular form. In addition, a modified temperature parameter, which approximately accounts for the effects of differential pressure and variations in panel skin material and skin thickness, is derived and used in conjunction with a flutter parameter to summarize the data as a flutter boundary which indicates the overall effects of compressive stress and buckling. The experimental data for flat, clamped panels are compared with results from an exact theory for the condition of zero midplane stress. In addition, a two-mode "transtability" solution for clamped panels is compared with the experimentally determined transition point.

SYMBOLS

$$\bar{A} = \frac{N_x}{\pi^2 \frac{D}{l^2}} - \frac{8}{3}\left(\frac{l}{w}\right)^2$$

C_1 constant (see eq. (A7))

c specific heat of panel material

D	panel flexural rigidity, $\frac{E\tau^3}{12(1 - \mu^2)}$
E	Young's modulus
f	frequency of flutter
h	aerodynamic heat-transfer coefficient
K_s	panel support factor, $\frac{12(1 - \mu^2)}{\pi^2(\beta_x - \mu)}$
k_x, k_y	spring constants per unit length (see fig. 12)
l	panel length (longitudinal direction, parallel to air flow)
M	Mach number
$N_x = \sigma_x \tau$	
p_∞	free-stream static pressure
p_b	static pressure in bay behind panel
Δp	differential pressure acting on panel skin, $p_b - p_\infty$
q	dynamic pressure
T	temperature
T_{aw}	adiabatic wall temperature
T_i	initial temperature of panel
T_t	stagnation temperature
T_∞	free-stream temperature
ΔT	average increase of panel skin temperature
t	time
t_i	time at which panel becomes exposed to airflow
w	panel width (lateral direction, perpendicular to airflow)

x coordinate, parallel to airflow (see fig. 12)

y coordinate, perpendicular to air flow (see fig. 12)

α coefficient of thermal expansion of panel skin

$\beta = \sqrt{M^2 - 1}$

$\beta_x = 1 + \frac{2E\tau}{l k_x}$

$\beta_y = 1 + \frac{2E\tau}{w k_y}$

γ_x average difference in arc length and chord length of panel in x-direction, $\frac{1}{2w} \int_0^w \int_0^l \left(\frac{\partial \delta}{\partial x}\right)^2 dx\, dy$

γ_y average difference in arc length and chord length of panel in y-direction, $\frac{1}{2l} \int_0^l \int_0^w \left(\frac{\partial \delta}{\partial y}\right)^2 dy\, dx$

δ vertical deflection of panel skin

η_r recovery factor, $\frac{T_{aw} - T_\infty}{T_t - T_\infty}$

μ Poisson's ratio

ρ specific weight of panel material

σ_x average midplane stress in x-direction, positive in compression

σ_y average midplane stress in y-direction, positive in compression

τ thickness of panel skin

Ψ modified temperature parameter, $\pm K_s \left\{ \pm\alpha\, \Delta T \left(\frac{l}{\tau}\right)^2 - 0.92 \left[\frac{\Delta p}{E}\left(\frac{l}{\tau}\right)^4\right]^{2/3} \right\}$

TESTS

Panels

The panels, which were 25.6 inches long and 26.6 inches wide, consisted of flat sheets of 0.072- or 0.081-inch-thick 2024-T3 aluminum alloy or 0.050-inch-thick 17-7 PH stainless steel riveted to Z-section stiffeners along the longitudinal and lateral edges. The stiffeners were approximately 1.6 inches deep and were formed from 0.125-inch-thick 2024-T3 aluminum alloy. Steel bars and angles were attached to the bottom of the stiffeners to provide support for mounting instrumentation. A rear-view photograph of a typical panel is shown in figure 1, and pertinent panel construction details are given in figure 2.

Test Apparatus

Langley 9- by 6-foot thermal structures tunnel.- All tests were conducted in the Langley 9- by 6-foot thermal structures tunnel, a Mach 3 intermittent blowdown facility exhausting to the atmosphere. A heat exchanger is preheated to provide stagnation temperatures up to 660° F and the stagnation pressure can be varied from 60 to 200 pounds per square inch absolute. (Additional details regarding the tunnel may be found in ref. 5.)

Panel holder and mounting arrangement.- The panels were mounted in a panel holder which extended vertically through the test section (fig. 3). The panel holder has a beveled half-wedge leading edge, flat sides, and a recess 29 inches wide, 30 inches high, and approximately 3.5 inches deep for accommodating test specimens. The recess is located on the nonbeveled side of the panel holder. Pneumatically operated sliding doors protect test specimens from aerodynamic buffeting and heating during tunnel starting and shutdown. Aerodynamic fences prevent shock waves emanating from the doors from interfering with the airflow over the test specimen. (The flow conditions over the area of the recess are essentially free-stream conditions as determined from pressure surveys of a flat calibration panel (ref. 5).) A vent-door arrangement on the side opposite the recess for the panel is used to control the pressure inside the chamber behind the test specimen.

All panels were mounted flush with the flat surface of the panel holder. (See fig. 3.) The panels were attached to a mounting fixture (bolted to the panel holder) by means of 0.125-inch-thick aluminum-alloy angles to provide support along the edges. (See fig. 4.) This mounting arrangement, which allowed partial thermal expansion of the panel skin in the longitudinal and lateral directions, was used in order to delay thermal buckling and thus permit more extensive study of the flat-panel boundary.

Instrumentation

Iron-constantan thermocouples, spotwelded to the panels at the 14 locations shown in figure 5, were used to measure panel temperatures. Inductance-type deflectometers were used to determine panel skin deflections. The deflectometers

were located approximately 1/4 inch behind the panel skin at the four positions indicated in figure 5. In addition, high-speed 16-millimeter motion pictures provided supplementary data on panel behavior. Grid lines were painted on the panel skins for photographic purposes.

Quick-response, strain-gage-type pressure transducers were used to measure static pressures in the tunnel and at various locations on the panel holder and in the chamber behind the panels. Tunnel stagnation pressures were obtained from static pressures measured in the settling chamber. Stagnation temperatures were measured by total temperature probes located in the test section. For each test all temperature and pressure data for both the test panels and the tunnel operating conditions were recorded on magnetic tape. Deflection data were recorded on high-speed oscillographs.

Test Procedure

The tests were conducted at a Mach number of 3.0, at dynamic pressures from 1,500 pounds per square foot to 5,000 pounds per square foot, and at stagnation temperatures from 300° F to 660° F. The protective doors on the panel holder were opened after desired test conditions were established. The dynamic pressure was held constant during the first few seconds of all tests but was varied during the remainder of most tests. The usual procedure for varying the dynamic pressure was as follows: (a) if no flutter had occurred after a predetermined length of time, the dynamic pressure was increased in an attempt to initiate flutter; (b) if flutter had started and stopped, the dynamic pressure was increased in an attempt to restart flutter; (c) if the panel was fluttering near the end of a test, the dynamic pressure was decreased in an attempt to stop flutter. The differential pressure on the panels was controlled manually in order to keep the differential pressure as small as possible (usually less than 0.6 pound per square inch). The stagnation temperature was essentially constant during most of the tests but decreased slightly during the latter portions of some tests. The protective doors were closed 3 seconds prior to tunnel shutdown. The duration of test conditions varied between approximately 5 and 50 seconds.

RESULTS AND DISCUSSION

Seventeen tests were made in this investigation, fourteen on aluminum-alloy panels and three on steel panels. Flutter, initiated by an increase in panel skin temperature, dynamic pressure, or both, was observed in all tests. Pertinent data for all tests are given in table I. The data tabulated include the stagnation temperature T_t, dynamic pressure q, differential pressure Δp, the skin-temperature increase ΔT, and the frequency f at the start of large-amplitude flutter.

Panel Temperatures

At the beginning of a test the panel skin and supporting structure were essentially at the same temperature. Any temperature increase of the panels prior to opening the panel holder protective doors was usually insignificant. After a panel was exposed to the airstream, the skin temperature increased in a manner similar to the typical temperature histories shown in figure 6 (test 14). The top curve represents the average of thermocouples 4 to 10 and 14; individual temperatures were within 10° F of the average value. The temperature histories for thermocouples 1, 2, 3, 11, 12, and 13 indicate that there were appreciable lateral and longitudinal temperature gradients in the panel skin near the supporting structure and large temperature gradients in the supporting structure. However, these temperature variations were neglected in analyzing the test data and the average increase in temperature of thermocouples 4 to 10 and 14 was considered to be the temperature increase ΔT of the panel skin. For two tests (tests 9 and 13) all or most of the skin thermocouples were lost during testing. Hence, for these tests calculated temperatures, obtained by the same procedure as used in reference 5, were used. Temperatures were calculated from the equation (ref. 10)

$$T = T_{aw} - \left(T_{aw} - T_i\right)e^{\frac{-h(t-t_i)}{c\rho\tau}} \tag{1}$$

which neglects temperature variation through the skin, heat flow by conduction, and heat transfer by radiation. The aerodynamic heat-transfer coefficients were obtained from the turbulent-flow flat-plate theory presented in reference 11 by using initial free-stream flow conditions, a skin temperature equal to T_i, and a reference length equal to the distance from the leading edge of the panel holder to the center of the panel. Temperature calculations, using adiabatic wall temperatures obtained in the usual manner $\left(\left(T_{aw}\right)_{calc} = \eta_r\left(T_t - T_\infty\right) + T_\infty\right.$, where $\left.\eta_r \text{ is the turbulent-flow recovery factor}\right)$, gave skin temperatures higher than the measured temperatures. An arbitrary adjustment of the adiabatic wall temperature was therefore made by using the relation

$$\left(T_{aw}\right)_{adj} = 0.90\left(T_{aw}\right)_{calc} \tag{2}$$

Use of this entirely empirical relationship in equation (1) resulted in fairly good agreement between measured and calculated temperatures. Figure 6 shows a comparison of measured and calculated temperatures for a typical test (test 14).

Flutter Parameters

The flutter data obtained in this investigation are summarized in terms of a dimensionless flutter parameter and a dimensionless modified temperature

parameter. The flutter parameter $\left(\frac{q}{\beta E}\right)^{1/3}\frac{l}{\tau}$ is proportional to the cube root of the primary panel flutter parameter given by theory (see, for example, ref. 7) and is the reciprocal of the parameter used in previous experimental investigations. (See, for example, refs. 5 and 6.) The dynamic pressure q, skin thickness τ, and Young's modulus E were varied in this investigation. Because of the short duration of the tests, changes in material properties with temperature were assumed to be negligible.

In this investigation the manual control of Δp resulted in differential pressure loadings of such magnitude that, when the data were plotted in terms of the parameter $\alpha\,\Delta T\left(\frac{l}{\tau}\right)^2$, as was done in reference 5, there was considerable scatter in the data, and thus it was desirable to consider the effects of Δp. Therefore, the effects of midplane stress and buckling are indicated, in terms of the temperature rise ΔT and the differential pressure Δp, by the modified temperature parameter ψ where

$$\psi = \pm K_s \left\{ \pm\alpha\,\Delta T\left(\frac{l}{\tau}\right)^2 - 0.92\left[\frac{\Delta p}{E}\left(\frac{l}{\tau}\right)^4\right]^{2/3} \right\} \tag{3}$$

In equation (3), which is derived in the appendix, the positive signs apply when a panel is flat inasmuch as ψ is then an indication of the stress ratio $\frac{N_x}{\pi^2 D/l^2}$ and may be positive (compression) or negative (tension) depending on the relative magnitudes of the temperature and differential pressure terms. However, when a panel is buckled, the negative signs apply inasmuch as the parameter ψ is then an indication of the buckle depth and both ΔT and Δp tend to increase the depth of buckle. (For this condition the panel is subjected to compressive stress and the negative sign in front of K_s insures that ψ will be positive.) The effects of the lateral and longitudinal inplane restraint of the supporting structure on the midplane stress are approximated through the support factor K_s. Values of K_s are listed in table I and were obtained from equation (A6); the appropriate stiffness of the supporting structure was represented by spring constants k_x and k_y (per unit length) which were obtained from an approximate analysis of the bending stiffness of the panel supporting structure and support angles.

Although theoretical investigations of the effects of midplane stress on panel flutter have used the ratio of midplane stress to Euler's buckling stress (for pinned ends) $\frac{N_x}{\pi^2 D/l^2}$, preference for the parameter ψ for this investigation resulted from several considerations. The skin-stiffener type construction and mounting arrangement used for the panels of this investigation permit restrained inplane and rotational displacements at the edges of the panel due to both thermal expansion of the skin and differential pressure loading. The resulting vertical displacements of the panel skin would necessitate use of nonlinear large deflection theory in conjunction with rather complicated boundary

conditions in order to determine the midplane stresses correctly. Rather than resort to such calculations, the parameter ψ, which gives an indication of the stress ratio $\frac{N_x}{\pi^2 D/l^2}$, was used to present the data.

Effects of Thermal Stress and Buckling on Panel Flutter

Results from all tests are presented in figure 7 in terms of the flutter parameter and the modified temperature parameter. When a panel was flat, flutter occurred initially as a large-amplitude motion that was periodic but nonharmonic. The open symbols in figure 7 represent the start of this large-amplitude flutter resulting from increasing thermal stress under either constant or increasing dynamic pressure. In most tests, the large-amplitude motion changed to small-amplitude flutter or an intermittent small-amplitude oscillation as the panel skin temperature increased. The half-solid symbols represent this transition from large-amplitude flutter to small-amplitude flutter. When the small-amplitude flutter stopped as a result of further heating or a reduction in dynamic pressure, the panels appeared to be buckled. The solid symbols represent this cessation of small-amplitude flutter. When a panel was thermally buckled at the start of flutter, the ensuing motion was of the small-amplitude type. The open symbols with tick marks represent the start of small-amplitude flutter from the buckled condition. Thus, as can be seen from figure 7, the overall boundary, faired through the experimental flutter points, consists of a flat-panel portion, a buckled-panel portion, and a transition point at the intersection of the two boundaries. The flutter region, which is above the boundaries, consists of two fairly distinct sections, a large-amplitude flutter region and a small-amplitude flutter region.

Flat-panel boundary and large-amplitude flutter region.- To the left of the transition point ($\psi < 16$) in figure 7, a panel is flat (unbuckled) when flutter starts. For a given panel and aerodynamic conditions, an increase in compressive thermal stress will make a flat panel more susceptible to flutter as indicated by the downward slope of the flat-panel boundary. Thus, as the value of the temperature parameter increases, the value of the flutter parameter required for flutter decreases until the transition point is reached. At the transition point, the value of the flutter parameter is a minimum (2.80) and is approximately 76 percent of the value for no stress (3.68).

The flutter-start points (panel flat) for the steel panels fall within the scatter of the data for the aluminum-alloy panels, as shown in figure 7. Thus, it appears that the flutter parameter $\left(\frac{q}{\beta E}\right)^{1/3}\frac{l}{\tau}$ and the modified temperature parameter ψ adequately account for variations in panel skin material and thickness, at least for the flat (unbuckled) panel data for these tests. Since the Δp term in the parameter ψ greatly reduced the scatter that resulted when Δp was neglected (see appendix), use of the term $\left[\frac{\Delta p}{E}\left(\frac{l}{\tau}\right)^4\right]^{2/3}$ appears to be justified as an approximation to the effects of Δp. Much of the remaining scatter in

the data probably results largely from the approximations used in calculating the effects of Δp and from the limitations imposed on ψ by neglecting certain factors such as edge rotation.

In all instances when a flat panel became unstable due to an increase in thermal stress, the resulting flutter consisted of large-amplitude motion that was periodic but nonharmonic. The initial motion was relatively steady when flutter started and the fundamental flutter frequency varied from 70 cycles per second to 140 cycles per second. The basic mode appeared to consist of a single half-wave in both the lateral and longitudinal directions. However, some higher frequency, lower amplitude motion was nearly always present as indicated in figure 8(a). (It should be noted that all deflectometers were located off center of the panel because the amplitude of the motion was so large that the panel skin could come in contact with deflectometers located near the center of the panel.) As a test progressed, the motion became more irregular as the higher frequency portion of the motion increased (fig. 8(b)). The irregular motion either continued to the end of the test or until there occurred a fairly distinct decrease in flutter amplitude (fig. 8(c)), which was usually accompanied by a change to a flutter mode consisting of several half-waves in one or both directions. The transition to small-amplitude flutter is indicated by the half-solid symbols in figure 7. As can be seen from the figure, the points representing the transition to small-amplitude flutter for the steel panels are in poor agreement with the data for the aluminum-alloy panels. This condition suggests that the parameter ψ does not account for variations in panel skin material for buckled panels.

Buckled-panel boundary and small-amplitude flutter region.- The solid boundary to the right of the transition point ($\psi > 16$, fig. 7) represents the buckled-panel flutter boundary, below which the panel is buckled and stable. As can be seen from the figure, the points representing the start of small-amplitude flutter (open symbols with tick marks) agree fairly well with the boundary established by the small-amplitude flutter stop points (solid symbols). The slope for the buckled boundary is reversed from that of the flat-panel boundary. This same reversal in trend has been shown experimentally for panels with length-width ratios of 10 (refs. 5 and 6) and theoretically by Fralich (contained in ref. 12) for a simply supported panel with length-width ratio of 1. The reversal in trend is attributed to the panel post-buckling behavior. Once a panel becomes thermally buckled, any additional temperature rise will increase the depth of buckle which tends to stiffen the panel (due to lateral curvature) as shown both theoretically and experimentally in terms of panel natural frequencies in references 13 and 14. In the stable buckled-panel region, and well to the right of the transition point, the buckling mode had either 1 or 3 half-waves in the longitudinal direction and 3 half-waves in the lateral direction (fig. 9).

The significance of the dashed boundary between the large-amplitude and small-amplitude flutter regions and the variations of panel flutter behavior within the small-amplitude flutter region are not clearly understood. To the left of the dashed boundary, the flutter mode always appeared to consist of a single half-wave in both the longitudinal and lateral directions, which corresponds to the fundamental buckling mode for square panels (for $\sigma_y/\sigma_x = 1.0$). To the right of the dashed boundary the flutter amplitude was small and the motion inconsistent. For several tests, flutter was observed to stop and then restart

(occasionally several times for a given test) within the small-amplitude flutter region. When flutter stopped, the panel appeared to be buckled. However, both the flutter and buckling modes were observed, at different times, to have 1, 2, or 3 half-waves in both the longitudinal and lateral directions. Usually the small-amplitude flutter consisted of low-frequency motion near the leading edge and high-frequency motion near the trailing edge but the motion did not appear to be entirely superimposed on the buckles. However, in some instances the motion consisted of very low-amplitude, high-frequency oscillations superimposed on the buckles or on a low-frequency oscillation of the buckles. In other tests the motion degenerated to a low-amplitude, intermittent oscillation that was aperiodic. In addition, short bursts of large-amplitude flutter, usually accompanied by an abrupt change in mode shape, were observed in the small-amplitude flutter region. In many instances, several of the different types of motion described above were observed in the small-amplitude flutter region during a given test.

These variations in flutter behavior within the small-amplitude flutter region appeared to be inconsistent and no definite trends could be established from the data available. Therefore, these variations in flutter behavior were not indicated in figure 7, and only those points used to establish the boundaries that define the small-amplitude flutter region are shown. One factor which probably contributed to the variations in panel-flutter behavior was the variations in buckling mode; variations in buckled mode shape have been shown experimentally (ref. 1) to affect the flutter characteristics of panels. Stein (refs. 15 and 16) has shown that increases in loading of buckled elastic structures (including rectangular plates) can result in changes in the buckled mode shape. Thus, the variations in panel flutter behavior suggest the possibility of additional buckled-panel boundaries within the small-amplitude flutter region. Moreover, the additional data and more thorough knowledge of the buckled mode shapes required to define these boundaries might also alter the boundaries shown in figure 7, which were arbitrarily faired through the data that defined the bounds of the small-amplitude flutter region.

That the boundary between the large-amplitude and small-amplitude flutter regions can be crossed from either side is suggested by the results of one test, as shown in figure 10. This figure shows the flutter boundaries of figure 7 and the variation of the flutter and modified temperature parameters during test 14 wherein the panel became thermally buckled prior to flutter. The panel, which was initially flat and stable, buckled in the vicinity of the transition point. (The buckle depth was so small that the number of half-waves could not be definitely ascertained.) The dynamic pressure was then increased and small-amplitude flutter started as indicated by the open symbol with tick mark. As the dynamic pressure continued to increase there occurred (near the dashed boundary) a transition from small-amplitude flutter to large-amplitude flutter and back to small-amplitude flutter, as indicated in figure 10. (The burst of large-amplitude flutter was not shown in fig. 7, since all other flutter points establishing the dashed boundary represented transition from large-amplitude flutter to small-amplitude flutter.)

One panel was damaged while undergoing small-amplitude flutter (test 13). The damage, which occurred approximately 6 seconds after flutter began, started as a tear along the inner rivet line at the trailing edge. This was quickly followed by several tears parallel to the airflow, which resulted in shredding of

the panel skin (fig. 11). The panel had previously been subjected to approximately 17 seconds of flutter (test 9).

Comparison with theory for conditions of zero stress and onset of buckling.- A theoretical flutter boundary, based on an exact solution for flat, finite, clamped panels subjected to midplane stress, is presented in reference 8 in terms of the parameters $\frac{2ql^3}{MD}$ and $\bar{A}$. However, the boundary of reference 8 extends only to $\bar{A} = -1$, whereas for the condition of zero stress for the panels of this investigation the value of $\bar{A}$ is -2.46. Thus it was necessary to make additional numerical calculations in order to extend the boundary of reference 8. The theoretical value of the flutter parameter so obtained for zero midplane stress was 3.40 (see fig. 7) which is 92 percent of the experimental value of 3.68 (in obtaining the theoretical value, the Mach number M, which appears in the parameter of ref. 8, was replaced by $\sqrt{M^2 - 1}$ which is applicable for a Mach number of 3.0).

Isaacs (ref. 17) introduced the concept of the "transtability" speed, a speed, calculated from purely static considerations, that constitutes the flutter speed of a panel at the onset of buckling. The transtability concept has been used in two mode analyses to determine the effects of the onset of buckling (which defines the transition point) on simply supported panels (ref. 7) and clamped panels (ref. 18). Reference 7 indicates that the value of the flutter parameter at the transition point depends on the stress ratio σ_y/σ_x; this ratio was estimated to be 1.0 for the panels of this investigation. The transition point for a square, clamped panel ($\sigma_y/\sigma_x = 1.0$) has been determined by the "transtability" method in reference 18 and found to be 2.20 (see fig. 7), which is approximately 79 percent of the experimental value of 2.80. The fact that the agreement between theory and experiment is not as good for the onset of buckling as for the condition of zero stress may be due to several factors. As the stress σ_x increases the effect of the differences in the actual and theoretical panel boundary conditions becomes more pronounced since the edge rotation induces vertical displacement (or curvature) of the panel skin. In addition, a two-mode analysis would be on the conservative side of the exact solution (refs. 7 and 8); in this case, a two-mode analysis increases the discrepancy between theory and experiment. In any event, it appears that the theory is conservative and is in fair agreement with experiment, at least for the panels of this investigation.

CONCLUSIONS

Flat, single-bay, skin-stiffener panels with length-width ratios of 0.96 were tested in the Langley 9- by 6-foot thermal structures tunnel to investigate the effects of thermal stress and buckling on the flutter characteristics of such panels. The tests were conducted at a Mach number of 3.0, at dynamic pressures ranging from 1,500 pounds per square foot to 5,000 pounds per square foot, and at stagnation temperatures from 300° F to 660° F. The panel supporting structure so restrained the panels that partial thermal expansion of the skins could occur in both the longitudinal and lateral directions. The ratio of the lateral to

longitudinal midplane stress in the panel skins was estimated to be approximately 1.0. The panel skins were 0.072- or 0.081-inch-thick aluminum alloy or 0.050-inch-thick stainless steel. A dimensionless modified temperature parameter, which approximately accounts for the effects of differential pressure and variations in panel skin material and skin thickness, was derived and used to indicate the flutter characteristics of thermally stressed panels. The tests revealed the following:

1. The overall flutter boundary consisted of a flat-panel portion, a buckled-panel portion, and a transition point between the two. The flutter trends indicated by the overall boundary were similar to the experimental trends obtained previously for panels with length-width ratios of 10 and to theoretical results obtained for simply supported panels with a length-width ratio of 1.0.

2. At the transition point, the value of the flutter parameter was a minimum and was approximately 76 percent of the value required for flutter of an unheated panel.

3. The flutter region consisted of two relatively distinct sections, a large-amplitude flutter region and a small-amplitude flutter region. Panel behavior in the large-amplitude flutter region consisted of periodic but nonharmonic motion. Panel flutter behavior in the small-amplitude flutter region was inconsistent. The variations in panel flutter behavior (in the small-amplitude flutter region) suggest the possibility of additional buckled-panel flutter boundaries within this region. For small-amplitude flutter, the panels usually appeared to be in a buckled condition.

4. The flat-panel (unbuckled) flutter data for the steel panels fell within the scatter of the data for the aluminum-alloy panels and indicated that the parameters used to summarize the data adequately account for variations in panel skin material and thickness.

5. Use of a differential pressure term in the modified temperature parameter greatly reduced the scatter in the data that resulted when the differential pressure Δp was neglected and thus the use of this term appears to be justified as an approximation to the effects of Δp.

6. Exact theoretical results for finite, clamped panels were in fair agreement with the experimental results for the condition of zero midplane stress. A two-mode "transtability" solution for clamped panels (for the onset of buckling) was in fair agreement with experiment at the transition point.

Langley Research Center,
National Aeronautics and Space Administration,
Langley Station, Hampton, Va., July 25, 1962.

APPENDIX

DERIVATION OF MODIFIED TEMPERATURE PARAMETER

As noted in the section entitled "Flutter Parameters," a dimensionless temperature parameter (modified to include the influence of differential pressure) is used to show the effects of both aerodynamic heating and differential pressure on the flutter data. The analysis herein uses stress-displacement relationships to relate panel midplane stress to temperature (see, for example, ref. 8) but employs a semiempirical approach for the inclusion of the effects of differential pressure.

Consider the idealized rectangular panel shown in figure 12. The panel edges are not permitted to deflect out of their original plane and longitudinal and lateral expansion is restrained by springs (with spring constants k_x and k_y per unit length, respectively) which represent the appropriate stiffness of the supporting structure. The panel skin is assumed to be subjected to a uniform temperature increase ΔT, thermal expansion of the supporting structure is assumed to be negligible, and a uniform differential pressure Δp acts on the panel so as to produce vertical displacement δ. Under these conditions, prior to buckling, compatibility in the x- and y-directions requires that

$$\frac{\sigma_x T}{k_x} = \frac{l}{2}\left(\alpha\,\Delta T + \frac{\mu}{E}\sigma_y - \frac{1}{E}\sigma_x\right) - \frac{\gamma_x}{2} \tag{A1a}$$

and

$$\frac{\sigma_y T}{k_y} = \frac{w}{2}\left(\alpha\,\Delta T + \frac{\mu}{E}\sigma_x - \frac{1}{E}\sigma_y\right) - \frac{\gamma_y}{2} \tag{A1b}$$

Solving equations (A1) for the average midplane stresses σ_x and σ_y yields

$$\sigma_x = E\left[\frac{\alpha\,\Delta T\left(\beta_y + \mu\right) - \left(\mu\frac{\gamma_y}{w} + \beta_y\frac{\gamma_x}{l}\right)}{\beta_x\beta_y - \mu^2}\right] \tag{A2a}$$

and

$$\sigma_y = E\left[\frac{\alpha\,\Delta T\left(\beta_x + \mu\right) - \left(\mu\frac{\gamma_x}{l} + \beta_x\frac{\gamma_y}{w}\right)}{\beta_x\beta_y - \mu^2}\right] \tag{A2b}$$

where

$$\beta_x = 1 + \frac{2E\tau}{lk_x} \tag{A3a}$$

and

$$\beta_y = 1 + \frac{2E\tau}{wk_y} \tag{A3b}$$

If it is assumed that the panel is square ($l = w$) and that $k_x = k_y$, then $\beta_x = \beta_y$, and $\gamma_x = \gamma_y$ and equation (A2a) may be written

$$\sigma_x = \frac{E}{\beta_x - \mu}\left(\alpha\,\Delta T - \frac{\gamma_x}{l}\right) \tag{A4}$$

Substitution of equation (A4) into the frequently used dimensionless stress ratio (the ratio of midplane stress in the direction of airflow to Euler's buckling stress for pinned ends) yields

$$\frac{N_x}{\pi^2 D/l^2} = K_s\left(\alpha\,\Delta T - \frac{\gamma_x}{l}\right)\left(\frac{l}{\tau}\right)^2 \tag{A5}$$

where

$$K_s = \frac{12(1 - \mu^2)}{\pi^2(\beta_x - \mu)} \tag{A6}$$

An approximation to the effects of Δp can be obtained by considering only the direct effect of membrane stresses induced by Δp; this approach neglects such effects as the interaction of induced thermal stresses and vertical displacements. Thus, if it is assumed that the deflected shape is a function of Δp only, then, since γ_x is a function of the deflected shape, equation (A5) may be written

$$\frac{N_x}{\pi^2 D/l^2} = K_s\left[\alpha\,\Delta T\left(\frac{l}{\tau}\right)^2 - C_1 g(\Delta p)\right] \tag{A7}$$

In this expression $g(\Delta p)$ is a nondimensional function of Δp, upon which $\frac{N_x}{\pi^2 D/l^2}$ depends when $\Delta T = 0$, and C_1 is a proportionality constant that can be

determined from the experimental data. The form of the function $g(\Delta p)$ can be obtained from an analysis of the stress in a square membrance subjected to a uniformly distributed normal loading. (See ref. 19.) When this stress is substituted in the stress ratio, the stress ratio is seen to be proportional to the dimensionless parameter $\left[\frac{\Delta p}{E}\left(\frac{l}{\tau}\right)^4\right]^{2/3}$ and thus equation (A7) may be expressed as

$$\frac{N_x}{\pi^2 D/l^2} = K_s \left\{ \alpha \, \Delta T \left(\frac{l}{\tau}\right)^2 - C_1 \left[\frac{\Delta p}{E}\left(\frac{l}{\tau}\right)^4\right]^{2/3} \right\} \tag{A8}$$

The constant C_1, obtained from the flat-panel flutter data, was found to be 0.92.

The results of the present investigation are presented in terms of the two parameters on the right-hand side of equation (A8) rather than in terms of the stress ratio itself in order to emphasize the approximations used in evaluating the effects of both aerodynamic heating and differential pressure and in order not to imply that the midplane stresses were accurately evaluated. Thus, equation (A8) becomes

$$\psi = \pm K_s \left\{ \pm \alpha \, \Delta T \left(\frac{l}{\tau}\right)^2 - 0.92 \left[\frac{\Delta p}{E}\left(\frac{l}{\tau}\right)^4\right]^{2/3} \right\} \tag{A9}$$

The positive signs apply when a panel is flat as ψ is then an indication of the stress ratio $\frac{N_x}{\pi^2 D/l^2}$ and may be positive (compression) or negative (tension) depending on the relative magnitudes of the temperature and differential pressure terms. When a panel is buckled, the negative signs apply as the parameter ψ is then an indication of the buckle depth and both ΔT and Δp tend to increase the depth of buckle. (For this condition the panel is subjected to compressive stress and the negative sign in front of K_s insures that ψ will be positive.) The parameter ψ was arbitrarily chosen to present buckled-panel data in order to avoid an additional and more complicated analysis; moreover, use of the parameter ψ tended to reduce the scatter in the data for the buckled-panel boundaries.

The constant C_1 was determined as follows. All flutter start points (panel flat) were initially plotted in terms of the parameters $\left(\frac{q}{\beta E}\right)^{1/3} \frac{l}{\tau}$ and $K_s \alpha \, \Delta T \left(\frac{l}{\tau}\right)^2$. An arbitrary boundary was faired through the points for which Δp was small ($\Delta p \leq 0.08$) as shown in figure 13. Then the values of $\Delta\left[K_s \alpha \, \Delta T \left(\frac{l}{\tau}\right)^2\right]$, representing the differences between the flutter points (to the

right of the boundary) and the arbitrary boundary, were plotted against the appropriate values of the differential pressure parameter $\left[\frac{\Delta p}{E}\left(\frac{l}{\tau}\right)^4\right]^{2/3}$. Since $\Delta\left[K_s\alpha\ \Delta T\left(\frac{l}{\tau}\right)^2\right]$ is an indication of the contribution of Δp to the stress ratio $\frac{N_x}{\pi^2 D/l^2}$, $\Delta\left[K_s\alpha\ \Delta T\left(\frac{l}{\tau}\right)^2\right]$ might be expected to vary approximately linearly with $\left[\frac{\Delta p}{E}\left(\frac{l}{\tau}\right)^4\right]^{2/3}$. The method of least squares was used to obtain a straight line through the data; the slope of this line (0.90) gave a first approximation to the constant C_1. The experimental flutter points were replotted by using the parameters $\left(\frac{q}{\beta E}\right)^{1/3}\frac{l}{\tau}$ and $K_s\left\{\alpha\ \Delta T\left(\frac{l}{\tau}\right)^2 - 0.90\left[\frac{\Delta p}{E}\left(\frac{l}{\tau}\right)^4\right]^{2/3}\right\}$ to obtain a new boundary. Then values of $\Delta\left[K_s\alpha\ \Delta T\left(\frac{l}{\tau}\right)^2\right]$, representing the differences between the values of $K_s\alpha\ \Delta T\left(\frac{l}{\tau}\right)^2$ at the flutter points and the values of $K_s\left\{\alpha\ \Delta T\left(\frac{l}{\tau}\right)^2 - 0.90\left[\frac{\Delta p}{E}\left(\frac{l}{\tau}\right)^4\right]^{2/3}\right\}$ at the new boundary, were plotted against $\left[\frac{\Delta p}{E}\left(\frac{l}{\tau}\right)^4\right]^{2/3}$ to obtain a final value for C_1 of 0.92 as shown in figure 14.

Use of the parameter ψ (with the aforementioned change in sign) tended to reduce the scatter in the buckled-panel data to the extent that reasonable flutter boundaries defining the small-amplitude flutter region could be established; thus, this procedure was not performed for the buckled-panel data and the value of C_1 of 0.92 was used in the parameter ψ to present all flutter data.

REFERENCES

1. Sylvester, Maurice A., and Baker, John E.: Some Experimental Studies of Panel Flutter at Mach Number 1.3. NACA TN 3914, 1957. (Supersedes NACA RM L52I16.)

2. Sylvester, Maurice A., Nelson, Herbert C., and Cunningham, Herbert J.: Experimental and Theoretical Studies of Panel Flutter at Mach Numbers 1.2 to 3.0. NACA RM L55E18b, 1955.

3. Sylvester, Maurice A.: Experimental Studies of Flutter of Buckled Rectangular Panels at Mach Numbers From 1.2 to 3.0 Including Effects of Pressure Differential and of Panel Width-Length Ratio. NASA TN D-833, 1961. (Supersedes NACA RM L55I30.)

4. Eisley, Joe Griffin: Panel Flutter in Supersonic Flow. Ph.D. Thesis, CIT, 1956.

5. Dixon, Sidney C., Griffith, George E., and Bohon, Herman L.: Experimental Investigation at Mach Number 3.0 of the Effects of Thermal Stress and Buckling on the Flutter of Four-Bay Aluminum Alloy Panels With Length-Width Ratios of 10. NASA TN D-921, 1961.

6. Guy, Lawrence D., and Bohon, Herman L.: Flutter of Aerodynamically Heated Aluminum-Alloy and Stainless-Steel Panels With Length-Width Ratio of 10 at Mach Number of 3.0. NASA TN D-1353, 1962.

7. Hedgepeth, John M.: Flutter of Rectangular Simply Supported Panels at High Supersonic Speeds. Jour. Aero. Sci., vol. 24, no. 8, Aug. 1957, pp. 563-573, 586.

8. Houbolt, John C.: A Study of Several Aerothermoelastic Problems of Aircraft Structures in High-Speed Flight. Nr. 5, Mitteilungen aus dem Institut für Flugzeugstatik und Leichtbau. Leemann (Zürich), c.1958.

9. Movchan, A. A.: On the Stability of a Panel Moving in a Gas. NASA RE 11-21-58W, 1959.

10. Heldenfels, Richard R., Rosecrans, Richard, and Griffith, George E.: Test of an Aerodynamically Heated Multiweb Wing Structure (MW-1) in a Free Jet at Mach Number 2. NACA RM L53E27, 1953.

11. Lee, Dorothy B., and Faget, Maxime A.: Charts Adapted From Van Driest's Turbulent Flat-Plate Theory for Determining Values of Turbulent Aerodynamic Friction and Heat-Transfer Coefficients. NACA TN 3811, 1956.

12. Garrick, I. E., and Cunningham, Herbert J.: Problems and Developments in Aerothermoelasticity. Proceedings of Symposium on Aerothermoelasticity, ASD Tech. Rep. 61-645, U.S. Air Force, 1961, pp. 12-60.

13. Bisplinghoff, R. L., and Pian, T. H. H.: On the Vibrations of Thermally Buckled Bars and Plates. Tech. Rep. 25-22, Office of Naval Res., Sept. 1956.

14. Shulman, Yechiel: On the Vibration of Thermally Stressed Plates in the Pre-Buckling and Post-Buckling States. Tech. Rep. 25-25, Office of Naval Res., Jan. 1958.

15. Stein, Manuel: The Phenomenon of Change in Buckle Pattern in Elastic Structures. NASA TR R-39, 1959.

16. Stein, Manuel: Loads and Deformations of Buckled Rectangular Plates. NASA TR R-40, 1959.

17. Isaacs, R. P.: Transtability Flutter of Supersonic Aircraft Panels. U.S. Air Force Project RAND P-101, The Rand Corp., July 1, 1949.

18. Leonard, Robert W., and Hedgepeth, John M.: Status of Flutter of Flat and Curved Panels. NACA RM L57D24c, 1957.

19. Timoshenko, S., and Woinowsky-Krieger, S.: Theory of Plates and Shells. Second ed., McGraw-Hill Book Co., Inc., 1959, p. 420.

TABLE I.- PANEL FLUTTER DATA

Skin material	τ, in.	E, psi	α, in./in.-°F	μ
2024-T3 aluminum alloy . .	0.081, 0.072	10.5×10^6	12.6×10^{-6}	0.3
17-7PH steel	0.050	29.5×10^6	6.1×10^{-6}	0.3

Test	τ, in.	K_s	T_t, °F	Flat panel				Buckled panel								
				Large-amplitude flutter start				Transition to small-amplitude flutter			Small-amplitude flutter stop			Small-amplitude flutter-start		
				q, psf	Δp, psi	ΔT, °F	f, cps	q, psf	Δp, psi	ΔT, °F	q, psf	Δp, psi	ΔT, °F	q, psf	Δp, psi	ΔT, °F
1	0.081	0.206	500	4,450	0.67	86	---	4,450	0.06	136	------	-----	---	------	-----	---
2	.081	.206	450	3,560	.02	43	120	3,580	-.20	62	3,600	-0.32	140	[a]4,550	-0.56	197
3	.081	.206	400	[a]4,510	.44	87	75	4,860	-.31	121	------	-----	---	------	-----	---
4	.081	.206	550	4,120	.08	59	80	4,120	-.29	72	[b]3,700	-.29	237	------	-----	---
5	.081	.206	660	------	----	--	---	-----	----	---	[a]4,210	-.57	167	[a]3,930	-.53	145
6	.072	.234	660	4,980	.48	41	110	5,010	-.37	135	[b]3,990	-.32	320	------	-----	---
7	.072	.234	400	[a]3,680	-.43	67	140	4,080	-.45	107	------	-----	---	------	-----	---
8	.072	.234	600	4,380	-.38	26	85	4,440	-.34	114	4,420	-.47	220	------	-----	---
9	.072	.234	450	3,780	-.10	53	75	3,780	-.40	109	[b]3,460	-.25	225	------	-----	---
10	.072	.234	660	4,710	.44	44	115	4,710	.04	143	4,700	.11	309	------	-----	---
11	.072	.234	320	3,570	-.03	42	80	-----	----	---	------	-----	---	------	-----	---
12	.072	.234	640	------	----	--	---	4,200	.11	131	4,200	.08	302	------	-----	---
13	.072	.234	500	------	----	--	---	-----	----	---	------	-----	---	[a]3,290	-.35	168
14	.072	.234	350	------	----	--	---	-----	----	---	------	-----	---	[a]2,050	-.04	80
15	.050	.234	450	4,270	.0	19	70	4,280	.0	158	------	-----	---	------	-----	---
16	.050	.122	550	3,930	.10	39	95	3,930	-.03	178	------	-----	---	------	-----	---
17	.050	.122	450	2,930	.08	62	---	2,930	.09	168	------	-----	---	------	-----	---

[a]Dynamic pressure increasing.
[b]Dynamic pressure decreasing.

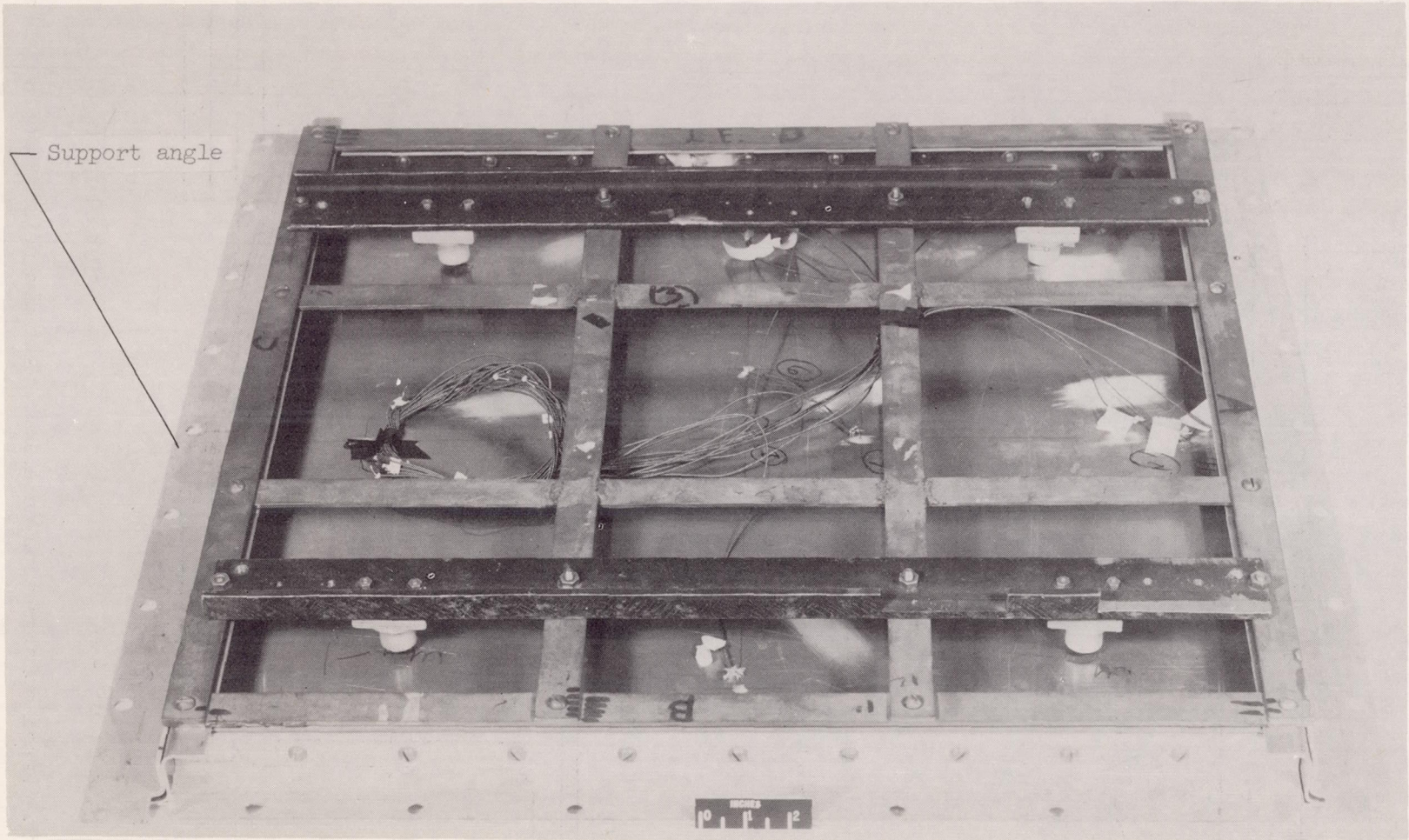

L-61-5745.1

Figure 1.- Back view of typical panel (with support angles attached).

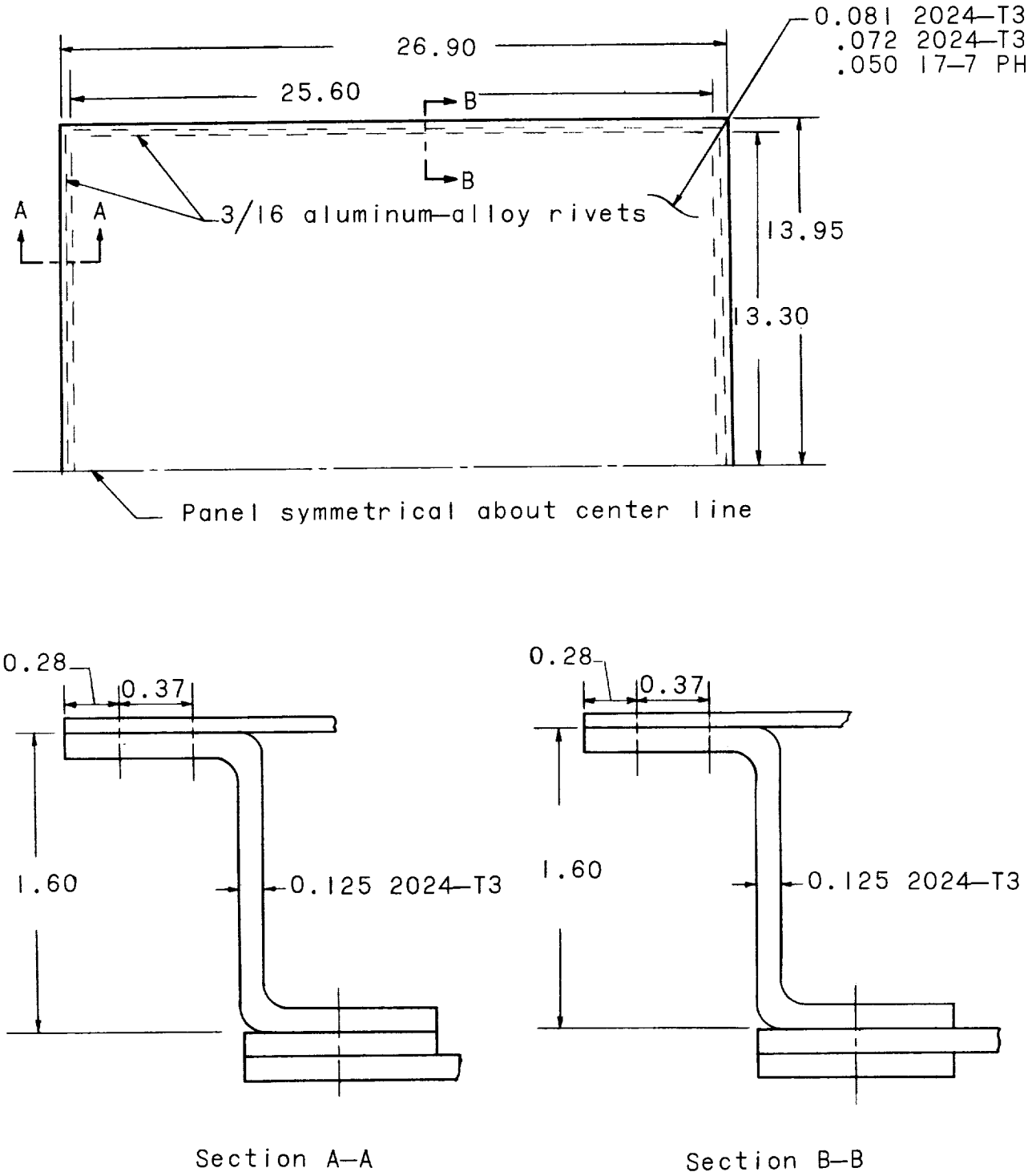

Figure 2.- Panel construction details. (All dimensions are in inches.)

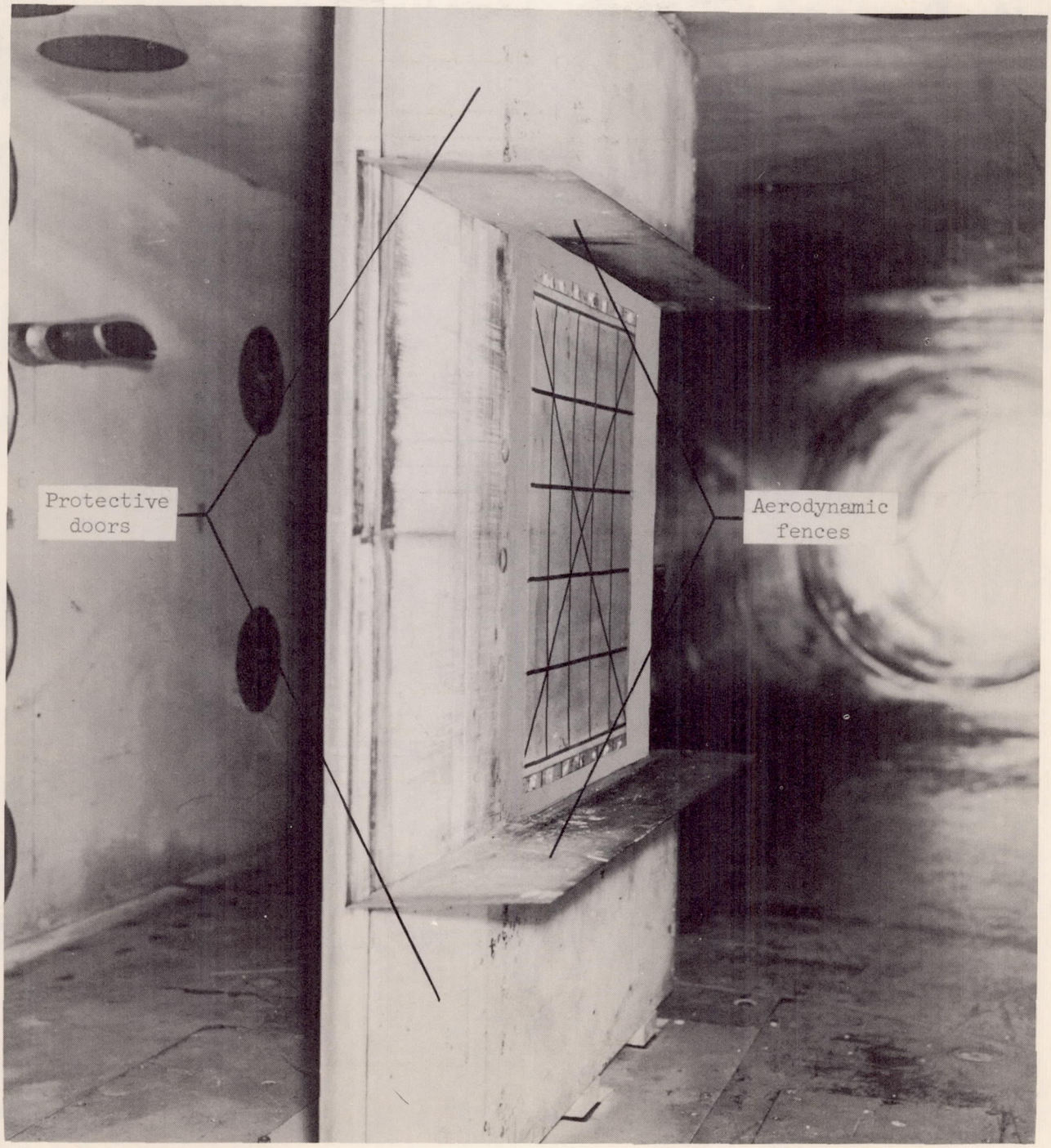

L-61-3962.1

Figure 3.- Panel mounted in panel holder in test section as viewed from upstream. Panel holder protective doors are in open position.

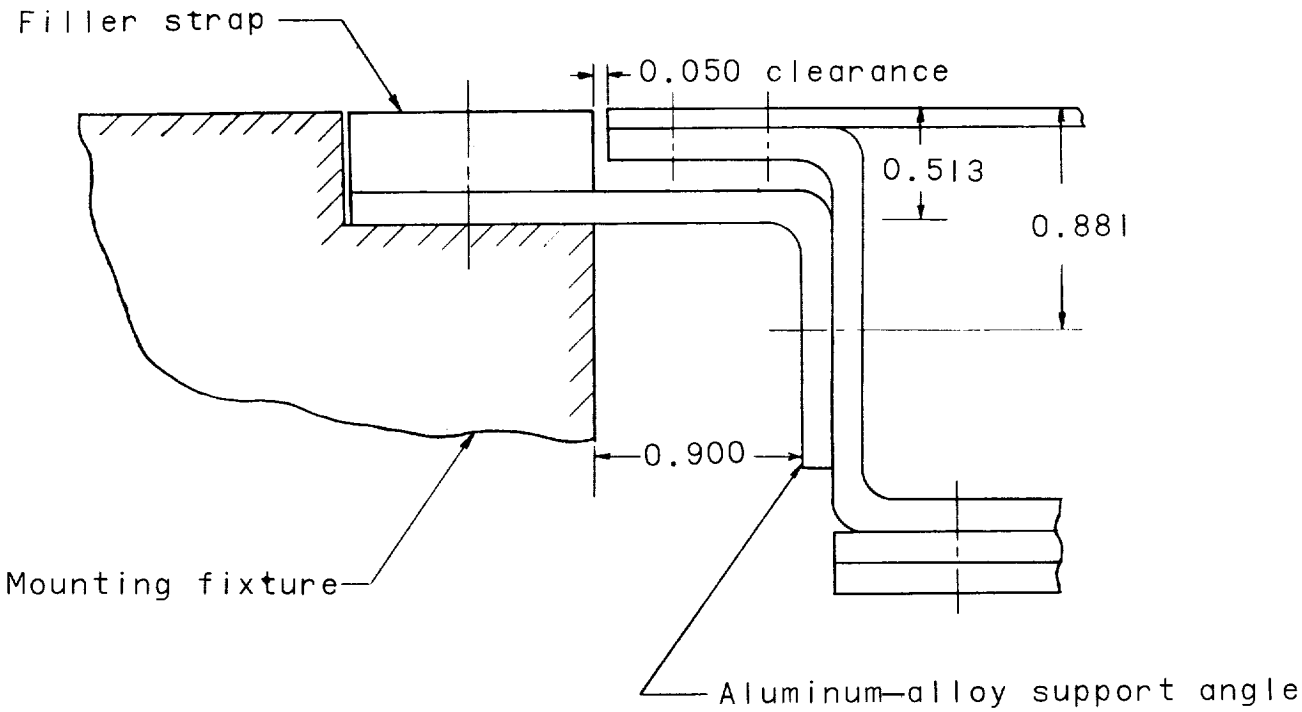

Figure 4.- Panel mounting detail. Typical for all edges.

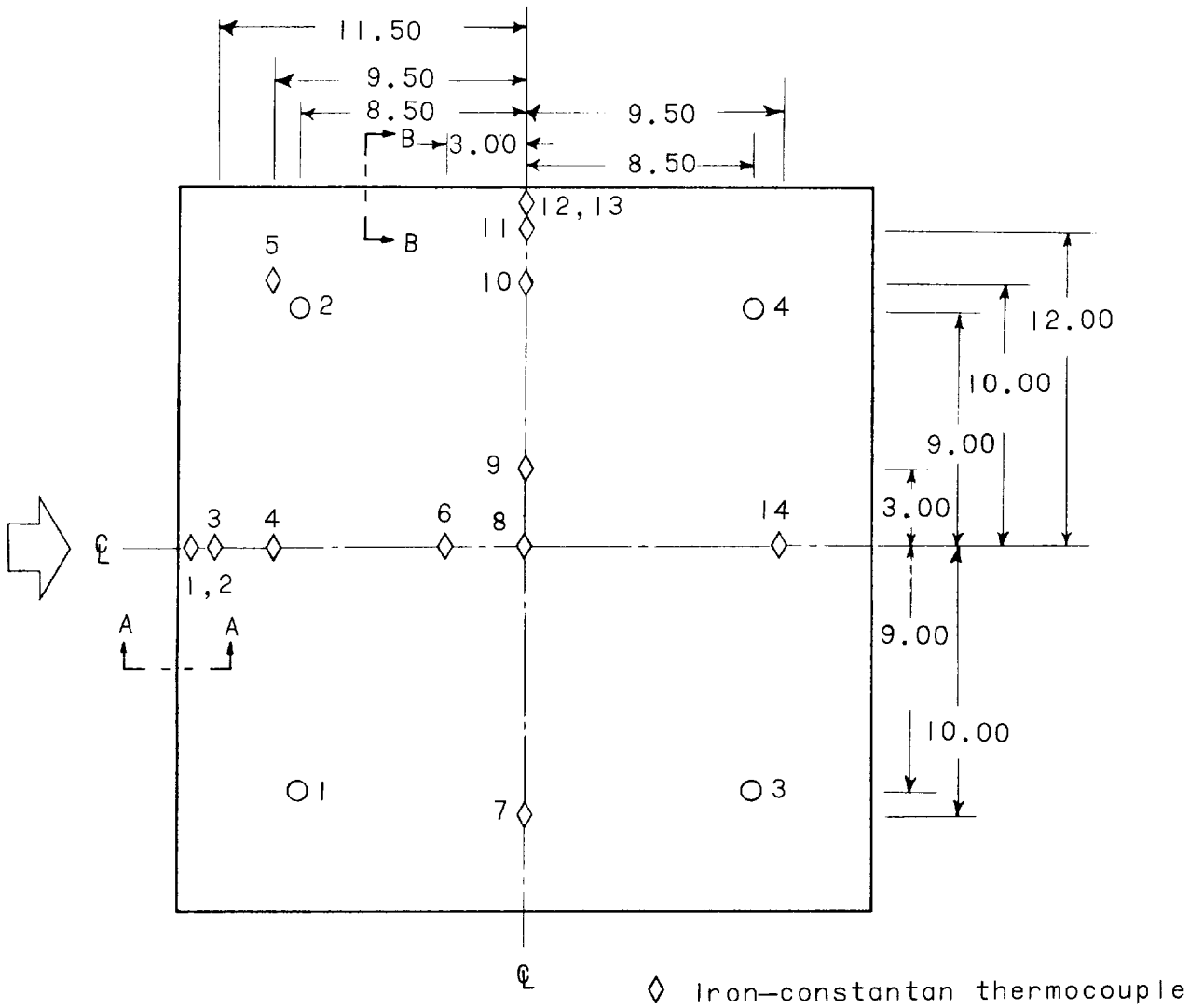

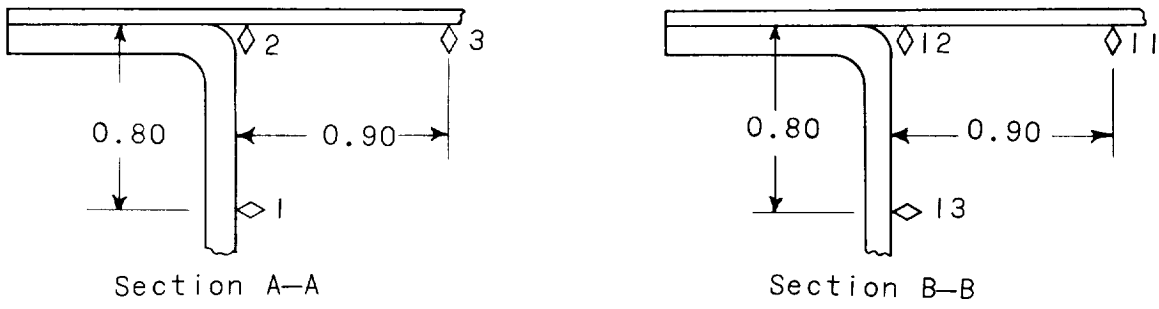

Figure 5.- Location of panel instrumentation (typical for all panels). All dimensions are in inches.

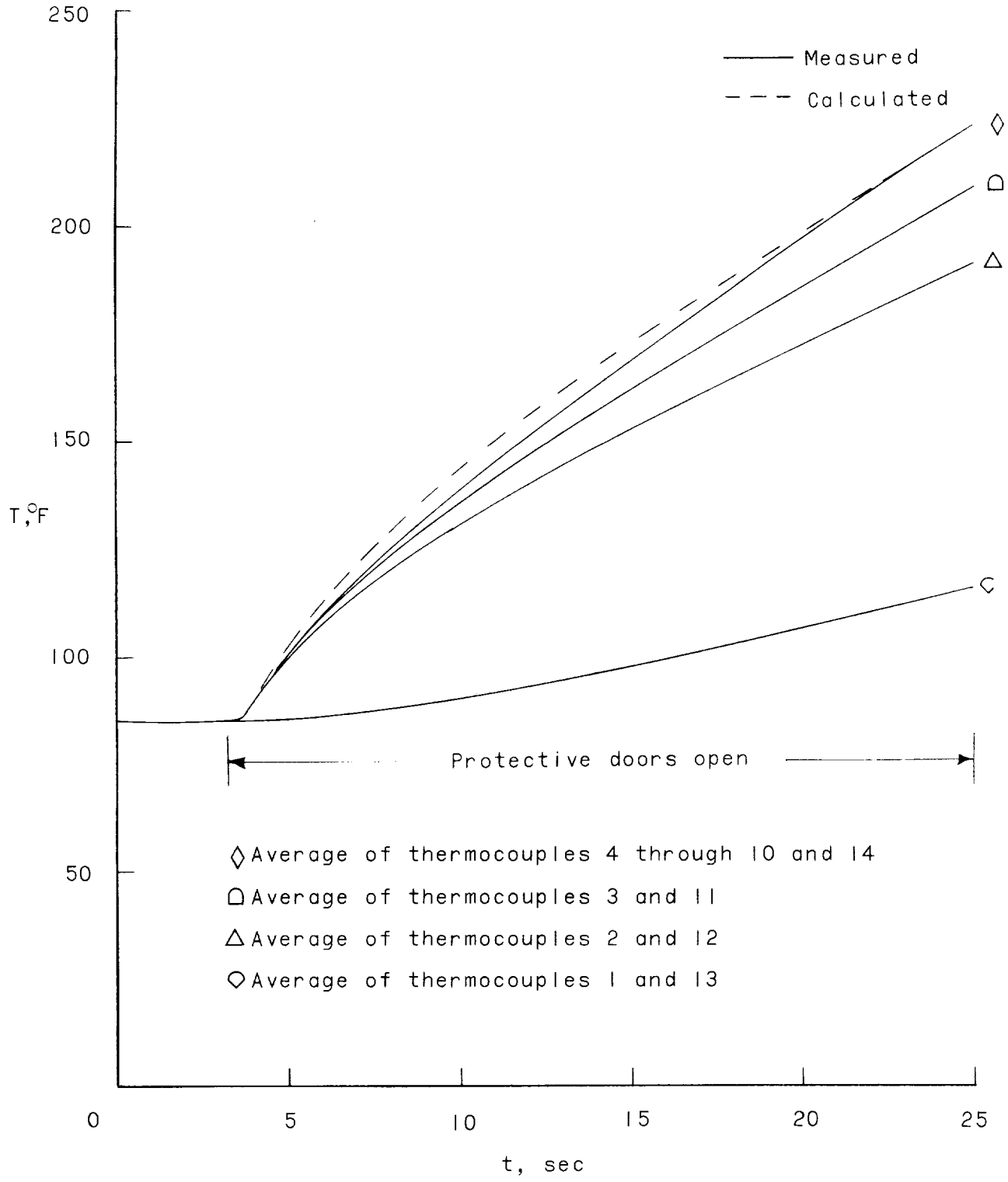

Figure 6.- Measured and calculated panel temperatures for test 14.

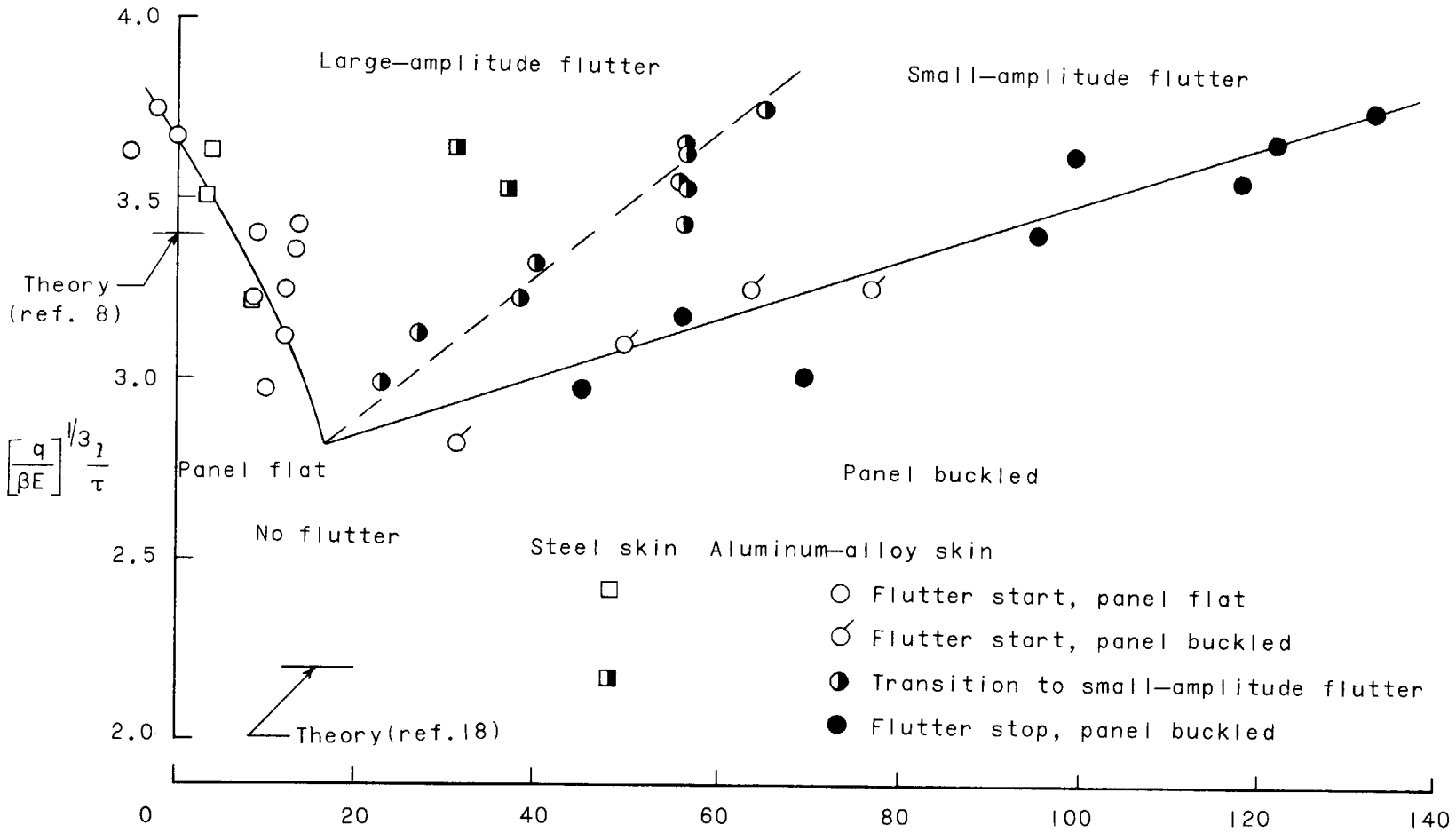

$$\psi = \pm K_s \left\{ \pm \alpha \Delta T \left(\frac{l}{\tau}\right)^2 - .92\left[\frac{\Delta p}{E}\left(\frac{l}{\tau}\right)^4\right]^{2/3} \right\}$$

Figure 7.- Effects of thermal stress and buckling on the flutter characteristics of panels with length-width ratios of 0.96. Positive signs in the expression for ψ apply when panel is flat, negative signs when panel is buckled. (See appendix.)

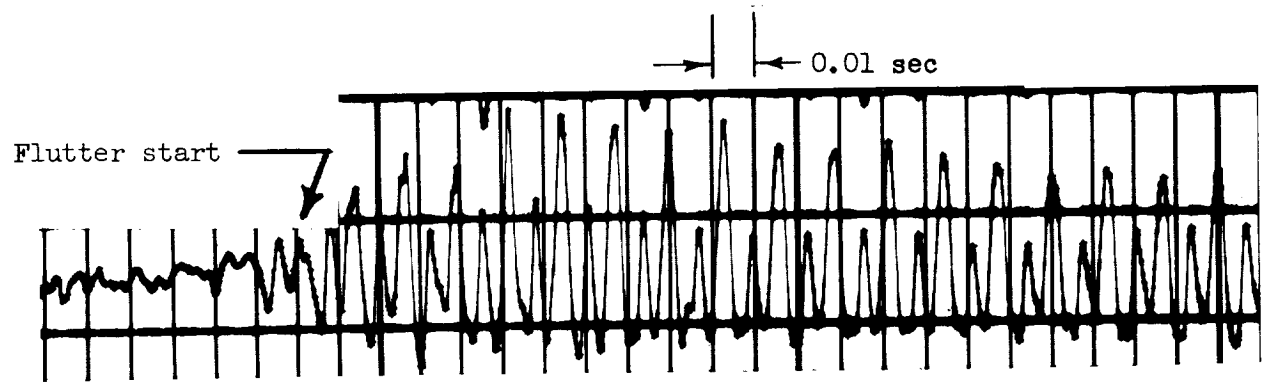

(a) Start of large-amplitude flutter under constant dynamic pressure (panel flat).

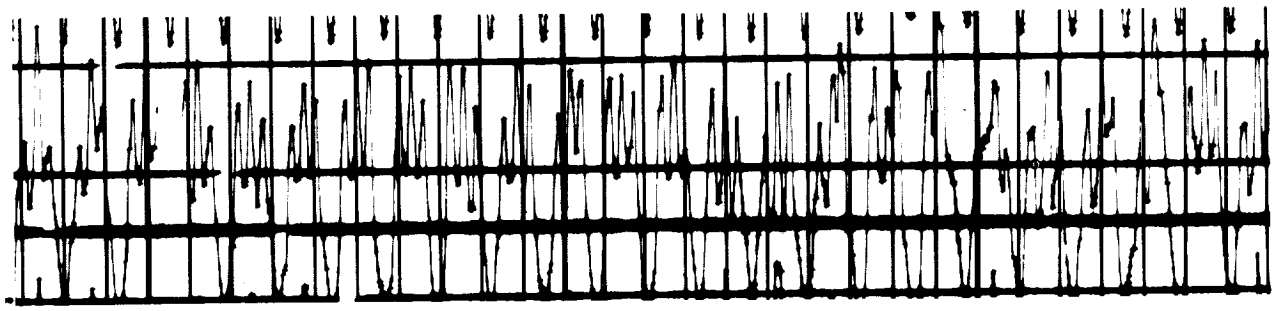

(b) Irregular large-amplitude flutter.

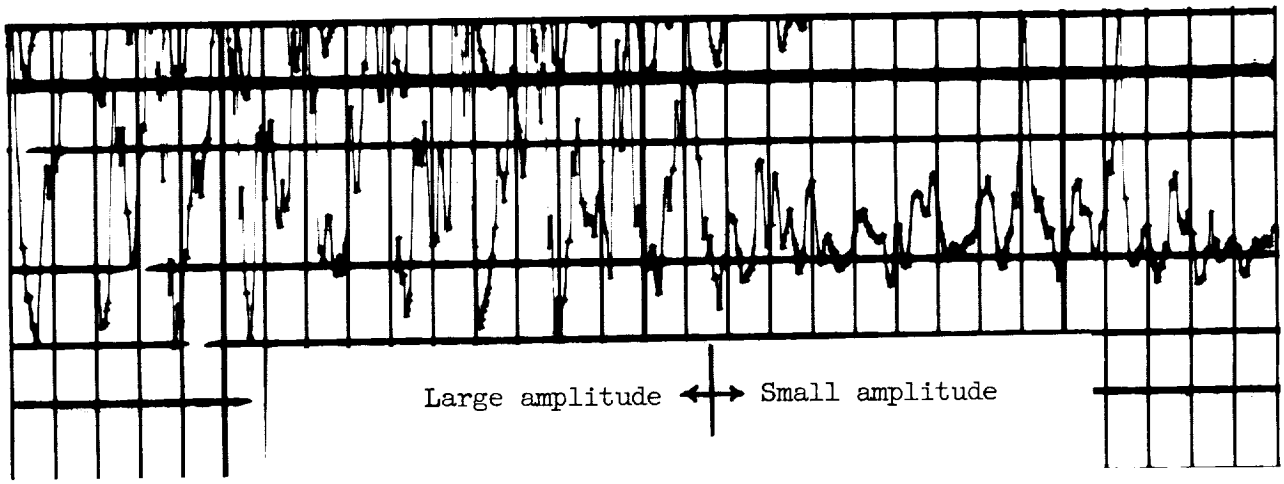

(c) Transition to small-amplitude flutter under constant dynamic pressure.

Figure 8.- Sample deflectometer records.

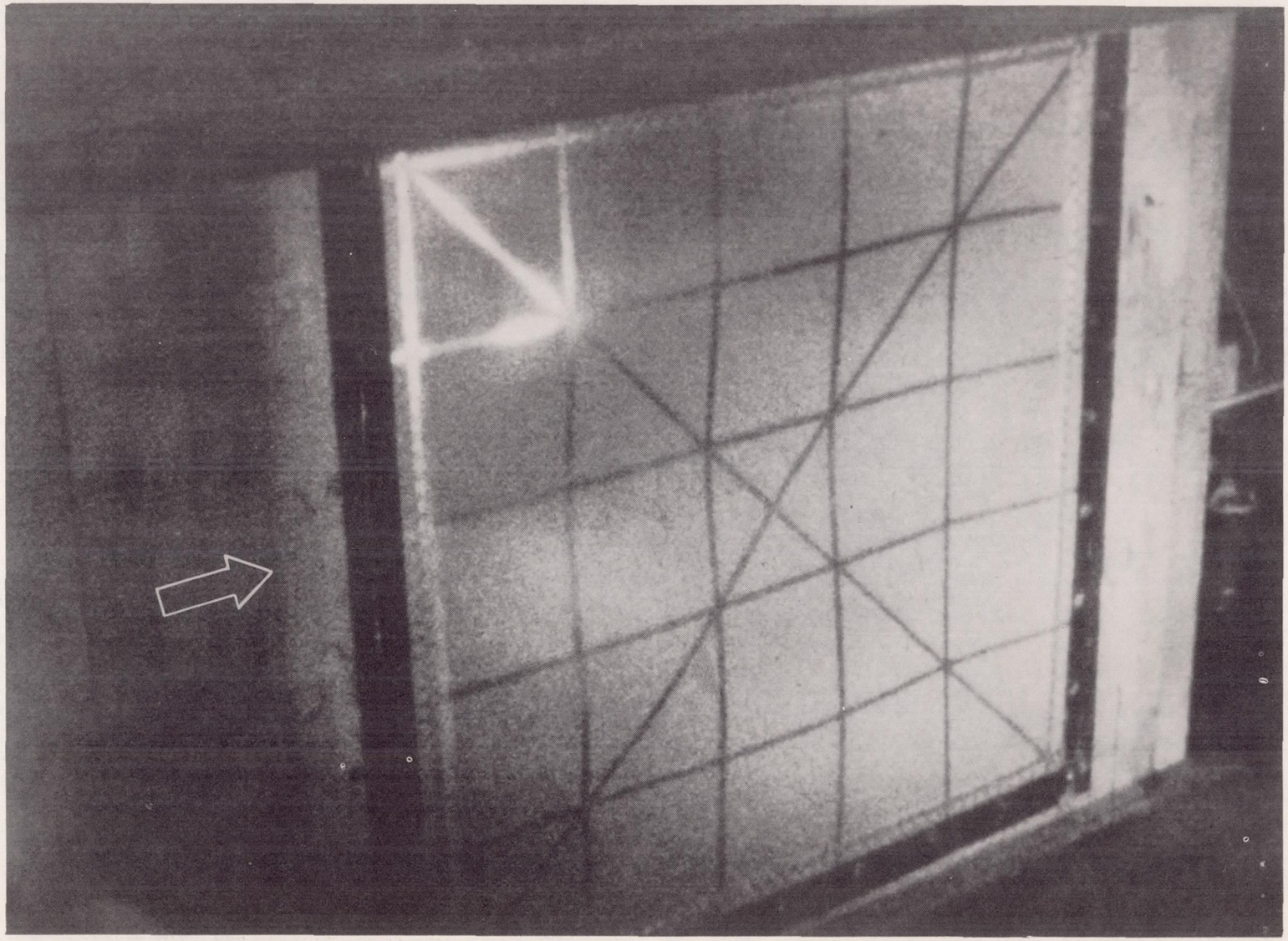

L-62-2122

Figure 9.- Panel buckled mode shape at cessation of small-amplitude flutter (test 8).

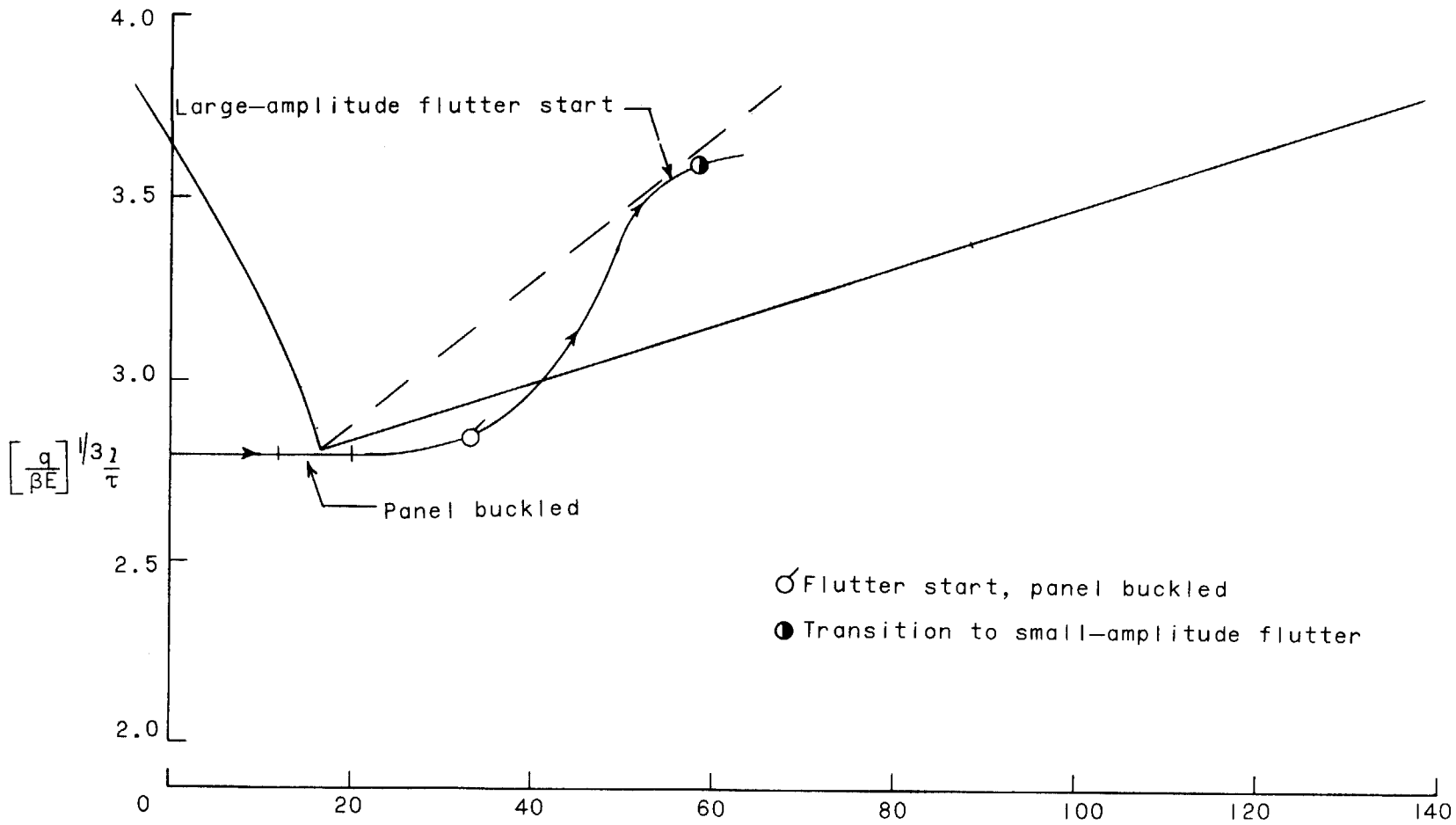

$$\psi = \pm K_s \left\{ \pm \alpha \Delta T \left(\frac{l}{\tau}\right)^2 - .92\left[\frac{\Delta p}{E}\left(\frac{l}{\tau}\right)^4\right]^{2/3} \right\}$$

Figure 10.- Variation of flutter and modified temperature parameter during test in which the panel was thermally buckled prior to flutter. Positive signs in the expression for ψ apply when panel is flat, negative signs when panel is buckled. (See appendix.)

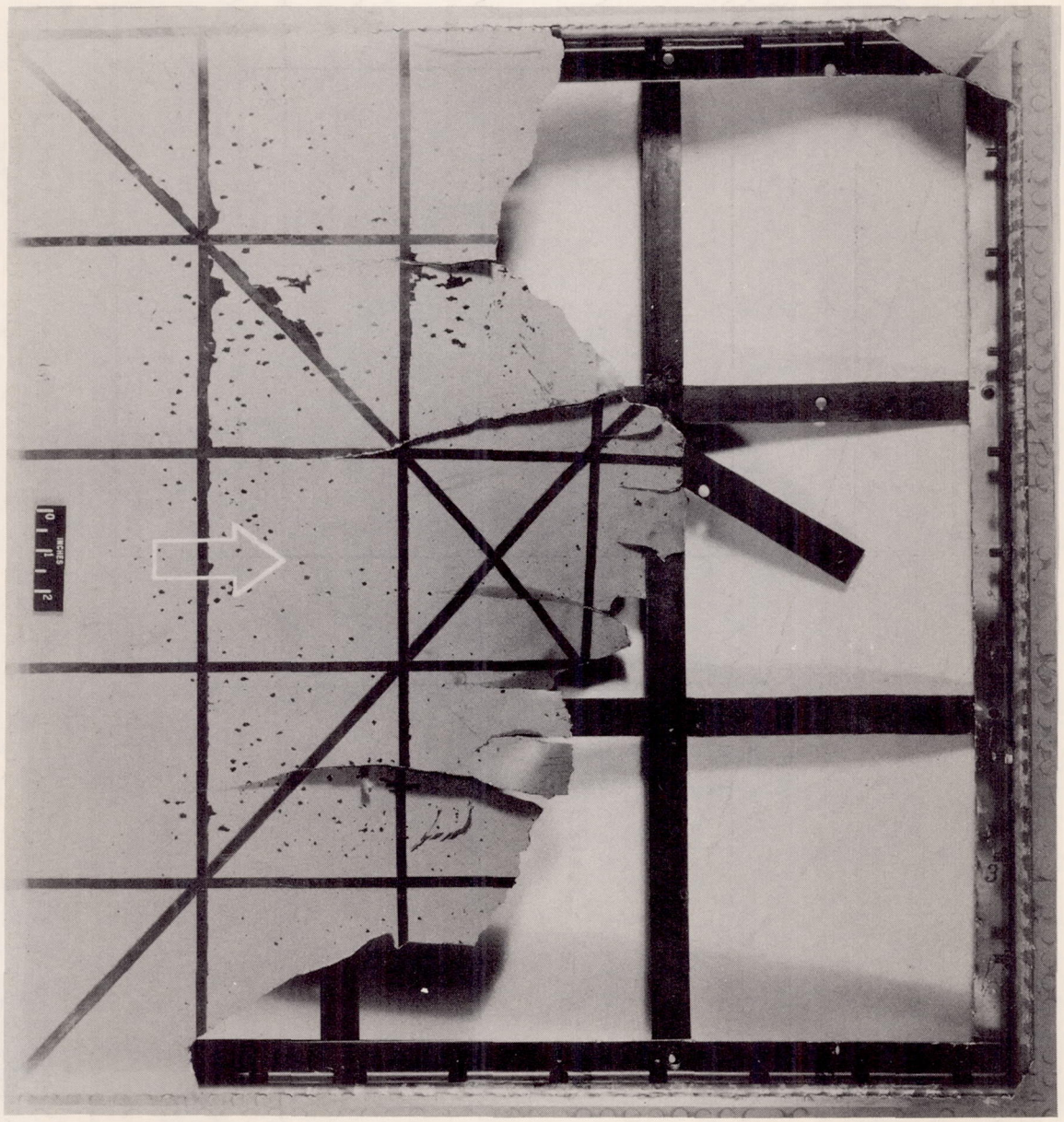

L-61-5744.1

Figure 11.- Damage to panel (downstream half) with 0.072-inch-thick aluminum-alloy skin after 6 seconds of flutter (test 13). Panel had previously fluttered for 17 seconds (test 9).

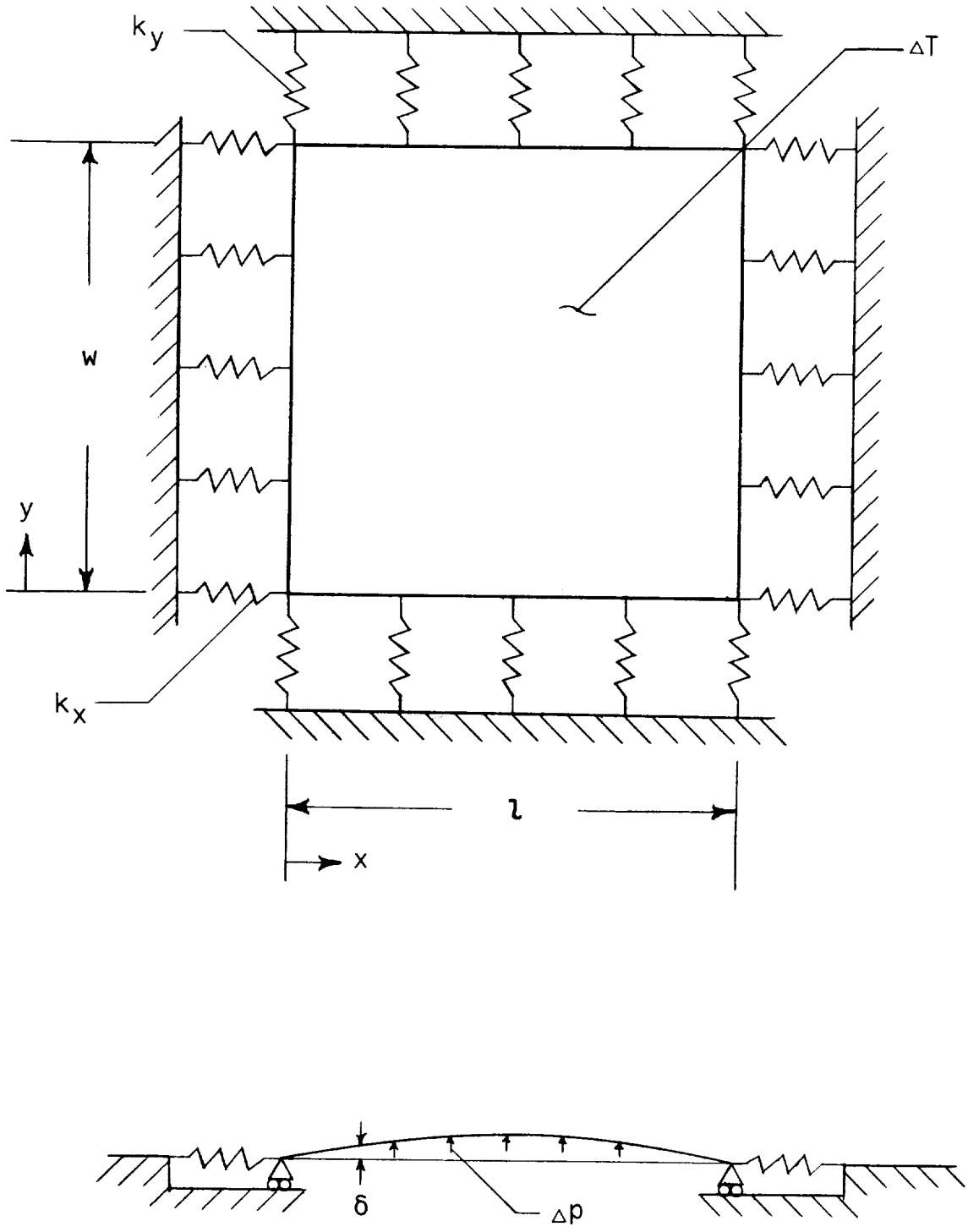

Figure 12.- Idealized panel configuration where panel is subjected to uniform temperature increase ΔT and uniform differential pressure Δp. Spring constants k_x and k_y represent effective stiffness of unheated supporting structure.

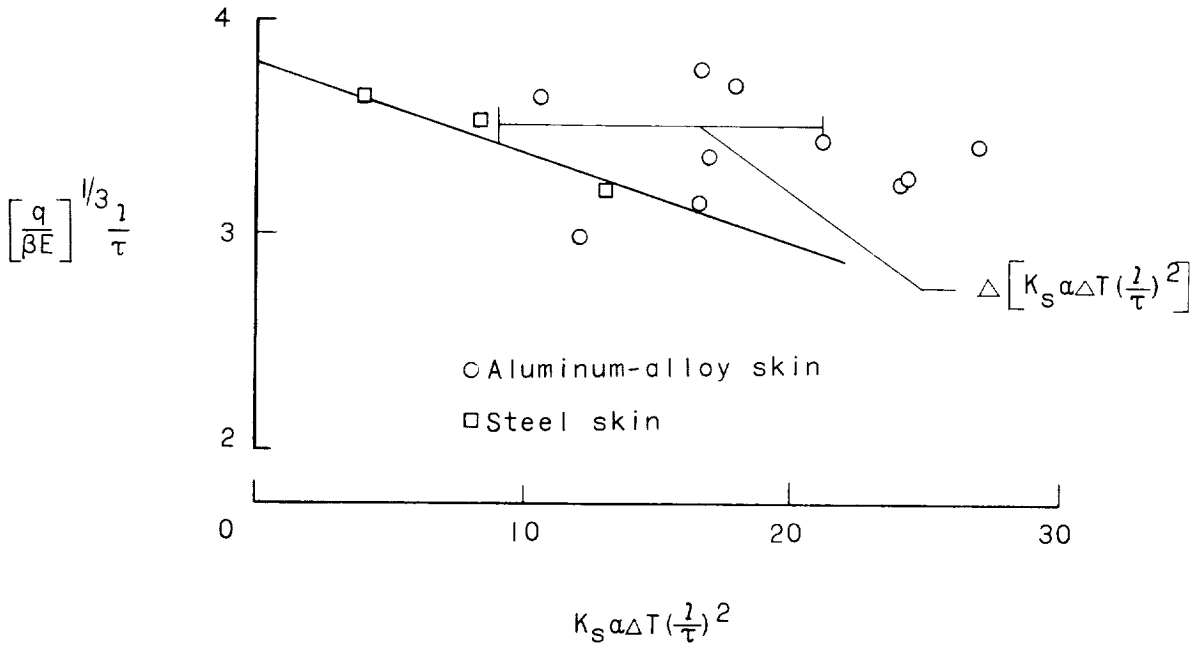

Figure 13.- Approximate flat-panel flutter boundary where data are unmodified for effects of differential pressure.

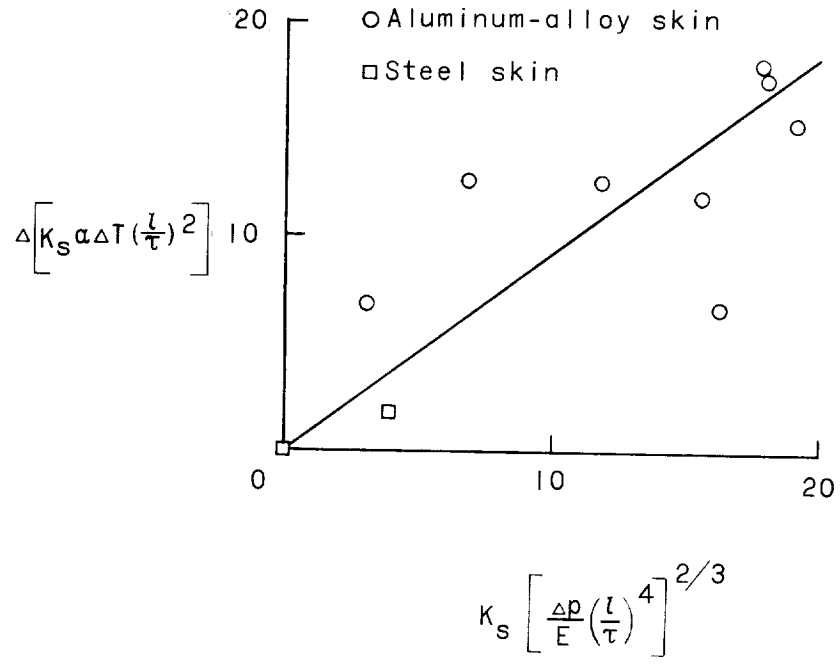

Figure 14.- Linear variation of $\Delta\left[K_s \alpha\, \Delta T \left(\frac{l}{\tau}\right)^2\right]$ with $K_s\left[\frac{\Delta P}{E}\left(\frac{l}{\tau}\right)^4\right]^{2/3}$.